Proc. Natl. Acad. Sci. USA
Vol. 93, pp. 8312–8317, August 1996
Biochemistry

The solution structure of the Raf-1 cysteine-rich domain: A novel Ras and phospholipid binding site

(signal transduction/nuclear magnetic resonance/zinc/protein kinase C)

HELEN R. MOTT*, JOHN W. CARPENTER*, SHENG ZHONG*, SUJOY GHOSH†, ROBERT M. BELL†, AND SHARON L. CAMPBELL*‡

*Department of Biochemistry and Biophysics, Lineberger Comprehensive Cancer Center, University of North Carolina, Chapel Hill, NC 27599; and †Glaxo Research Institute, Five Moore Drive, Research Triangle Park, NC 27708

Communicated by Alfred G. Redfield, Brandeis University, Waltham, MA, May 6, 1996 (received for review April 3, 1996)

ABSTRACT **The Raf-1 protein kinase is the best-characterized downstream effector of activated Ras. Interaction with Ras leads to Raf-1 activation and results in transduction of cell growth and differentiation signals. The details of Raf-1 activation are unclear, but our characterization of a second Ras-binding site in the cysteine-rich domain (CRD) and the involvement of both Ras-binding sites in effective Raf-1-mediated transformation provides insight into the molecular aspects and consequences of Ras–Raf interactions. The Raf-1 CRD is a member of an emerging family of domains, many of which are found within signal transducing proteins. Several contain binding sites for diacylglycerol (or phorbol esters) and phosphatidylserine and are believed to play a role in membrane translocation and enzyme activation. The CRD from Raf-1 does not bind diacylglycerol but interacts with Ras and phosphatidylserine. To investigate the ligand-binding specificities associated with CRDs, we have determined the solution structure of the Raf-1 CRD using heteronuclear multidimensional NMR. We show that there are differences between this structure and the structures of two related domains from protein kinase C (PKC). The differences are confined to regions of the CRDs involved in binding phorbol ester in the PKC domains. Since phosphatidylserine is a common ligand, we expect its binding site to be located in regions where the structures of the Raf-1 and PKC domains are similar. The structure of the Raf-1 CRD represents an example of this family of domains that does not bind diacylglycerol and provides a framework for investigating its interactions with other molecules.**

Raf-1 is a serine/threonine kinase whose activation is regulated by the action of extracellular signals such as hormones and mitogens (1). A critical step in the activation of Raf-1 is its interaction with membrane-anchored Ras, an oncoprotein found to be deregulated in many human tumors (reviewed in ref. 2). The activation of the Raf-1 kinase initiates the mitogen-activated protein kinase cascade, which transduces cellular growth and differentiation signals to the nucleus (3, 4). It has been shown that Ras-mediated translocation of Raf-1 to the plasma membrane is the first step of Raf activation, but Ras interaction alone is not sufficient to activate the Raf-1 kinase and other events, such as Raf-1 phosphorylation, may be required (5, 6).

Raf proteins contain several conserved regions (reviewed in ref. 1). At the carboxyl (C)-terminal end is the catalytic kinase domain that shows specificity for phosphorylation of serine and threonine residues. The amino (N)-terminal region of Raf-1 is thought to be involved in negative regulation of the kinase domain, since its removal or mutation can lead to tumorigenesis (7–9). Residues 55–131, in the N terminus of Raf-1, have been shown to constitute a Ras binding site (10, 11), termed Ras-binding site I (RBS-1). The structure of this domain and the identification of the Ras-interaction surface have recently been elucidated by nuclear magnetic resonance (NMR) (12), and the structure of RBS-1 in a complex with the Ras-related protein Rap1A has also been solved by x-ray crystallography (13). In addition, it has been shown that there is a second, distinct, binding site for Ras (RBS-2) within the conserved cysteine-rich domain (CRD) in the N-terminal region of Raf-1 (14, 15). This CRD encompasses residues 139–184. Results from our laboratory (16) suggest that interactions between Ras and both of these binding sites may be required for Raf-mediated transformation. Studies with full-length and truncated Raf-1 proteins, as well as various Ras mutants, have suggested that these two binding sites interact with distinct regions of Ras (16, 17), and that the RBS-2 may be cryptic in intact, unstimulated Raf-1 (18). The Raf-1 CRD has also been shown to be responsible for binding phospholipids (14) and possibly 14-3-3 proteins (19–24). The role of these interactions in Raf-1 activation is still unclear, although a plethora of data suggests that the CRD may be involved (25, 26).

There is no structural information available on Raf-1 residues 139–184. Sequence comparisons show that this domain is homologous to a family of CRDs (14), each of which bind two molecules of zinc. These CRDs are found in several other proteins involved in signal transduction such as protein kinase C (PKC) (27), N-chimaerin (28), diacylglycerol kinase (29), and Vav (30). In many of these proteins the CRD includes a binding site for diacylglycerol (DAG) and tumor-promoting phorbol esters (31), suggesting it may interact with the cell membrane. The association with lipid bilayers is further implicated by the demonstration that these CRDs also include binding sites for phosphatidylserine (PS). It is notable that the Raf-1 CRD does not bind DAG, even though it interacts with PS (14).

The structures of homologous CRDs from PKC α and δ, both of which bind DAG and phorbol esters, have recently been solved and shown to consist of two small β-sheets with a very short helix at the C terminus (32, 33). To investigate further the role of the CRD in Raf-1 activation, and the basis of the ligand specificities in this family of domains, we have determined its solution structure using two-dimensional (2D) and three-dimensional (3D) heteronuclear NMR methods. Here, we compare the structure of the Raf-1 CRD with the structures of the CRDs from PKC. We show that, although the overall topology of the molecules is similar, the second loop

The publication costs of this article were defrayed in part by page charge payment. This article must therefore be hereby marked "*advertisement*" in accordance with 18 U.S.C. §1734 solely to indicate this fact.

Abbreviations: COSY, correlation spectroscopy; CRD, cysteine-rich domain; 2D and 3D, two- and three-dimensional; DAG, diacylglycerol; NOE, nuclear Overhauser enhancement; NOESY, NOE spectroscopy; PKC, protein kinase C; PS, phosphatidylserine; RMSD, root mean squared deviation; TOCSY, total correlation spectroscopy.

‡To whom reprint requests should be addressed.

that is implicated in DAG and phorbol ester binding in the PKC domains has a very different structure in the Raf-1 domain. We suggest that these structural differences may account for the different binding specificities of these domains.

MATERIALS AND METHODS

Expression and Purification. Residues 136–187 from Raf-1 were expressed in *Escherichia coli* and purified as described (14). Pure protein in 30 mM Tris·acetate, pH 6.2/75 mM Na_2SO_4/10 μM $ZnCl_2$/1 mM DTT was concentrated to 1 ml using an Amicon ultrafiltration stirred cell, containing a YM-1 membrane (Amicon) then exchanged into NMR buffer (30 mM d_{11}-Tris·d_3-acetate, pH 6.2/75 mM Na_2SO_4/10 μM $ZnCl_2$/1 mM d_{10}-DTT/10% D_2O/0.01% NaN_3) using a Pharmacia PD-10 gel filtration column. Finally, samples were concentrated in a Centricon-3 (Amicon) to a final concentration of 0.5-1.0 mM in a volume of 550 μl. ^{15}N-labeled protein was obtained by growing *E. coli* with 99.8% $^{15}NH_4Cl$ as the sole nitrogen source. D_2O (^2H_2O) samples were obtained by exchanging the protein twice, using the Pharmacia PD-10 column, into NMR buffer that had been made up with 99.9% D_2O.

NMR Spectroscopy. NMR experiments were recorded at 25°C on a Bruker (Billerica, MA) AMX500 spectrometer. A 3D ^{15}N-edited nuclear Overhauser enhancement (NOE) spectroscopy (NOESY) experiment (34) was recorded with sensitivity-enhanced coherence order selection using pulsed-field gradients (35), with a mixing time of 200 msec. A 3D ^{15}N-edited total correlation spectroscopy (TOCSY) experiment (36) was recorded utilizing DIPSI-3 (37) with a mixing time of 70 msec. Three-dimensional experiments were acquired as 512 × 96 × 48 complex points, with spectral widths of 6024.1, 1250.0, and 6024.1 Hz for the f1, f2, and f3 dimensions, respectively. Water suppression in the 3D TOCSY was achieved using Watergate (38) and purging gradients. Two-dimensional experiments were recorded on a sample in D_2O as follows: double quantum filtered correlation spectroscopy (DQF-COSY) (39), homonuclear TOCSY (40) with a 72 msec DIPSI-3 mixing time, NOESY experiments (41) with mixing times of 100 msec, 150 msec, and 200 msec. In these experiments the residual water was suppressed using low power saturation. The D_2O experiments were typically acquired as 1024 × 512 complex points (except the COSY experiments, which were recorded as 2048 × 512 complex points), with spectral widths of 6024.1 Hz in each dimension. NH-C$^\alpha$H coupling constants were identified from a series of 2D ^1H-^{15}N *J*-modulated COSY experiments (42), where the NH-C$^\alpha$H *J*-coupling was allowed to evolve for 10–110 msec, incremented in 10 msec steps in each successive experiment. The *J*-couplings were evaluated by fitting the cross-peak intensities as previously described (42), using a program provided by F. Moy. C$^\alpha$H-C$^\beta$H coupling constants were identified from a primitive exclusive COSY experiment (43) and these were used to estimate χ_1 angles in combination with NOESY experiments recorded with mixing times of 60 msec. Hydrogen bonds were identified by the presence of slowly exchanging amide protons in a 2D ^1H NOESY experiment that was recorded ≈20 hr after the sample was buffer-exchanged into D_2O. NMR data were processed and analyzed using the program FELIX, version 2.30 (Biosym Technologies, San Diego). In the 3D experiments, linear prediction was used in the indirect dimensions to double the number of complex points.

Structure Calculation. Structure calculations were performed using X-PLOR, version 3.1 (44), following the hybrid distance-geometry/simulated annealing protocol as described in the X-PLOR manual except that the high temperature dynamics was increased in length to 32 psec. A total of 602 NMR-derived restraints were used, including 553 NOE restraints, of which 119 were sequential, 41 were short-range (2–4 residues apart in sequence), and 141 were long-range (5 or more residues apart in the sequence). There were five pairs of hydrogen bonds identified from slowly exchanging amide protons, where the carbonyl donors were identified by examination of the initial structures that had been calculated on the basis of NOEs only. In addition, 28 ϕ restraints were identified from the J-modulated COSY experiment, where a coupling constant of >8 Hz was associated with a ϕ angle of $-139° \pm 30$, and a coupling constant of <6 Hz was associated with a ϕ angle of $-60° \pm 30$. There were also 11 χ_1 restraints measured from a combination of PE-COSY and 60 msec NOESY experiments recorded in H_2O and D_2O. The structure calculations were initially run with no Zn^{2+} restraints, and the identity of the Zn^{2+} binding residues could be inferred from their positions, as well as the homology to the CRDs from PKC. The histidine ring nitrogen involved in coordinating Zn^{2+} was identified by recording a ^{15}N-^1H heteronuclear single quantum correlation spectrum with a total ^1H-^{15}N evolution period of 22 msec, and the ^{15}N spectral frequency shifted by +5000 Hz relative to the regular ^{15}N frequency (45). The evolution period used ensured that direct ^1H-^{15}N couplings were minimized, and only the multi-bond couplings in the histidine ring were observed. The Zn^{2+} was then added and held in place by NOE distances of 2.3 Å for S-Zn^{2+} and 2.0 Å for N-Zn^{2+} (46).

RESULTS AND DISCUSSION

Secondary Structure and Topology. The 2D and 3D NMR datasets collected on the Raf-1 CRD enabled almost complete resonance assignment. The 3D ^{15}N-edited TOCSY experiment was used to correlate the backbone amide resonances with the intra-residue C$^\alpha$H and side-chain proton resonances and the 3D ^{15}N-edited NOESY spectrum was used to complete spin system identification and establish sequential connectivities. The spin system assignments were then extended using the 2D and 3D spectra (47). The residues whose resonances could not be assigned included the three N-terminal amino acids (Raf-1 residues 136–138), which are outside the consensus sequence for these domains, and the backbone amide protons of Leu-147 and Thr-178. Long-range NOEs were identified from both 2D and 3D NOESY experiments.

The protonation of the histidine nitrogens was assessed using the ^{15}N-^1H heteronuclear single quantum correlation as described in *Materials and Methods*. It was evident from the characteristic chemical shifts of the histidine nitrogen resonances in this spectrum and the 2- and 3-bond coupling constants within the histidine ring that the N$^{\varepsilon 2}$ was protonated and the N$^{\delta 1}$ was deprotonated under the sample conditions (48). Thus it is likely that the N$^{\delta 1}$ is the nitrogen involved in coordinating with Zn^{2+}, the same nitrogen as that observed in PKC. These results suggest that this scheme of Zn^{2+} coordination may be conserved in all CRDs.

The secondary structure of the Raf-1 CRD could be assigned on the basis of short- and medium-range NOEs and coupling constants, as summarized in Fig. 1. It is composed of 5 β-strands, encompassing residues 140–146, 150–151, 157–159, 161–165, and 170–173 and a region that has some helical character, encompassing residues 177–180. The backbone amide proton resonances of several residues within this helix are broad, suggesting that they are involved in chemical exchange. The helix is ill-defined by the short-range NOEs and coupling constants, but it is clearly present in the 3D structures; thus it is defined by long-range interactions involving the side-chains rather than the short-range interactions involving the backbone amide protons.

The overall topology of this domain can be inferred from the pattern of long-range NOEs as shown in Fig. 2 and from the representation of the structure shown in Fig. 3*A*. Thus, there are two β-sheets: the first comprises the first, fourth, and fifth

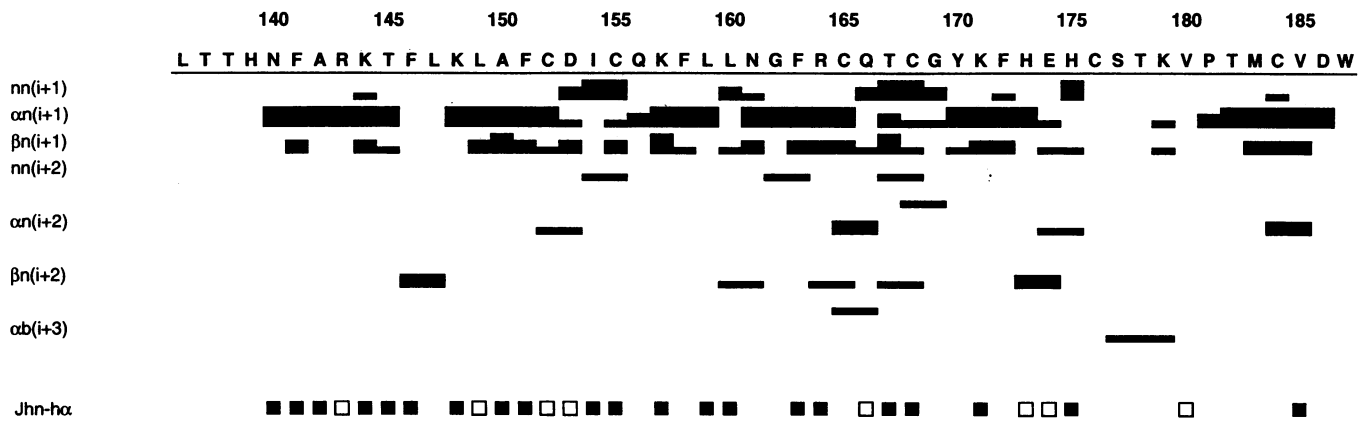

FIG. 1. Summary of the short-range NOEs and coupling constants observed for the Raf-1 CRD. NOEs were classified into strong, medium, and weak, and their strength is indicated by the width of the bar in each case. nn(i + 1) refers to a NOE between the backbone NH of residue i and the NH of residue i + 1. The other NOE types are represented in a similar way. Coupling constants of less than 6 Hz are represented by open squares and those of greater than 8 Hz by filled squares. This figure was generated with a program provided by Bruno Kieffer (University of Strasbourg).

β-strands and the second comprises the second and third β-strands. The C-terminal helix packs against the first β-strand, so that the N and C termini come together to form one Zn^{2+} binding site. The second Zn^{2+} binding site is formed from residues in the loop between the second and third β-strands and the loop between the fifth β-strand and the C-terminal helix. The structures are in good agreement with the experimental data, with no NOE violations more than 0.5 Å and no dihedral angle violations more than 5°. The root mean squared deviation (RMSD) over all backbone atoms within the consensus sequence for this motif is 0.92 Å. The residues outside the consensus sequence, 136–138 and 185–187, are disordered and are not included in the structural statistics.

Several regions of the structure exhibit flexibility, as judged from the RMSDs, and a decrease in the heteronuclear NOE (data not shown). One such region is the C-terminal helix. It appears that this helix is solvent-exposed with broad backbone amide resonances that prevented heteronuclear NOE measurements. These large linewidths also impeded the assignment of NOEs involving the backbone atoms in this helix. The

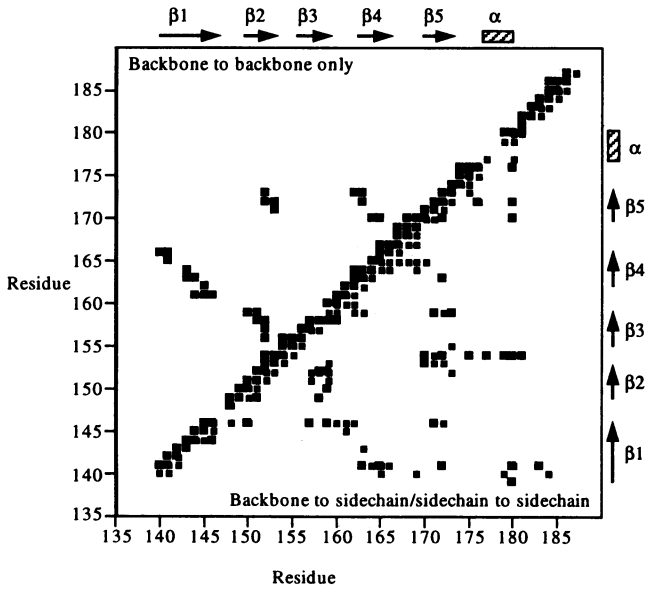

FIG. 2. Summary of all the NOEs assigned for the Raf-1 CRD in the form of a scatter plot. Each square represents a single NOE. The positions of the β-strands and α-helix are indicated.

lack of NOEs accounts for the high RMSD in this region, but whether this is due to conformational exchange or a high degree of solvent exposure is not clear. This mobility may be due to the excision of this domain from the full-length Raf-1 protein, since the extreme C terminus of this construct, residues 185–187, is disordered. Alternatively, since mobile regions in proteins are often involved in interactions with other molecules, the C-terminal helix of the Raf-1 CRD may be involved in ligand interactions. One of the other regions of flexibility encompasses residues 146–150, and the significance these residues will be discussed below. The RMSD of the backbone atoms decreases significantly, from 0.9 Å to 0.4 Å when these two mobile regions are removed from the calculation, as shown in Table 1.

Comparison of Raf-1 CRD with CRDs from PKC Reveals Structural and Dynamic Differences in a Ligand-Binding Region. A comparison with the CRDs from PKC α determined by NMR (32) methods and PKC δ determined by x-ray crystallography (33), shows that all three have a similar secondary structure. The sequence alignments and position of the secondary structural elements of all three domains are shown in Fig. 4. This shows that the lengths of the secondary structural elements are conserved between all three CRDs, and thus are likely to be similar in other members of the family, such as Vav and DAG kinase.

A combination of mutagenesis and structural work has identified the position of residues in PKC δ that interact with phorbol ester (33, 51). Competitive binding and mutagenesis data suggest that DAG and phorbol ester bind the same site in PKC (reviewed in ref. 52). The position of these residues is also identified in the sequence comparison, and it is apparent that one of the two regions of the sequence involved in phorbol ester binding to the PKC δ CRD corresponds to a deletion in the Raf-1 domain. Thus it is of interest to compare the 3D structures of the Raf-1 and PKC δ domains to determine the differences in these ligand-binding regions.

Fig. 5 shows a comparison of the x-ray crystal structure of the PKC δ CRD, complexed with phorbol ester (33), with the structure of the Raf-1 CRD. The first region of PKC δ that interacts with phorbol ester, the loop between β-strands 1 and 2, is very similar in the two CRDs, even though the sequences of the two domains are not conserved in this region. However, the second region, the loop between β-strands 3 and 4 is the position of this deletion in the Raf-1 domain. It is shorter than the corresponding loop in the PKC domains and some of the residues that interact with the phorbol ester in the PKC δ domain are not present in the Raf-1 domain. These differences in the structures of the second loop, combined with the lack of

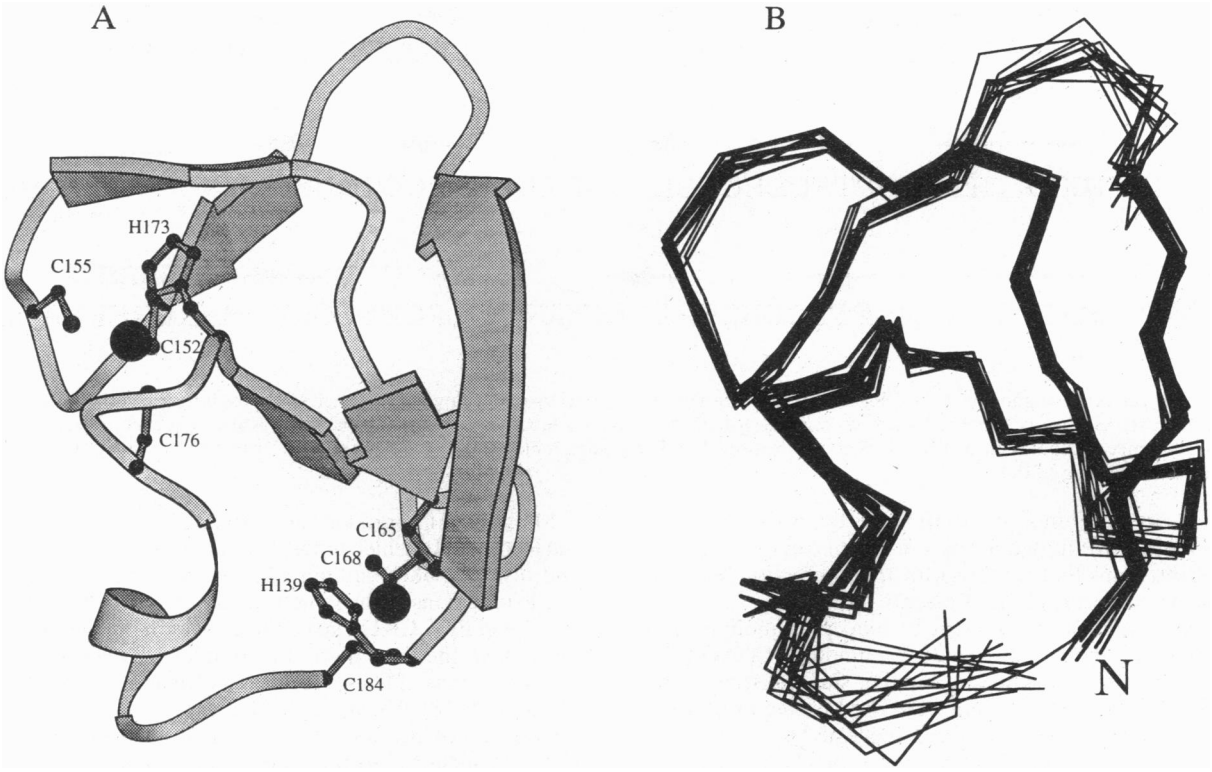

FIG. 3. (*A*) A ribbon representation of a typical structure of the CRD, with the Zn^{2+} ions illustrated as black spheres. The side chains corresponding to cysteine and histidine residues involved in Zn^{2+} coordination are also displayed. (*B*) A C^{α} trace showing 16 representative final structures, superimposed over all residues shown, in approximately the same orientation as in *A*. These figures were generated using MOLSCRIPT (49).

sequence conservation in the first loop, are a likely explanation for why the Raf-1 CRD does not bind to phorbol esters. The deletion in this loop of the Raf-1 CRD introduces more asymmetry in this region, so that the loop cannot form one side of the binding pocket.

A consensus sequence within the CRD of Raf-1 has been identified by sequence comparison of Raf and Ras-GTPase activating protein family members (50). This sequence in full-length Raf-1 is near the N terminus of the CRD, from Arg-143 to Ala-150, and is highlighted in Fig. 4. Peptides corresponding to this consensus sequence were found to inhibit Raf-1 dependent phosphorylation of mitogen-activated protein kinase (50). There is no direct evidence that this region of the domain interacts with Ras, but these residues may be involved in Raf-1 activation. Residues 146–150, within this consensus sequence, appear to be more mobile than the other loops, based on the convergence of the structures and the dynamics measurements, as discussed above. Interestingly, the corresponding loops in the PKC α NMR structure, that are thought to interact with DAG and phorbol esters, appeared to be less well-defined by the data. The binding of phorbol ester to these two loops in the PKC δ domain causes a shift in the relative orientations of the loops and pushes them apart by $\approx$0.4 Å. The shift in the orientation of these loops would be facilitated by their mobility. Since in the Raf-1 CRD only one of these loops appears to be mobile, their relative orientation cannot be changed in the same way as those in the homologous domain from PKC δ. This may be an additional factor in why Raf-1 cannot bind phorbol esters.

Implications for Interactions with Other Molecules. We have presented the structure of a CRD family member that does not bind DAG or phorbol esters. Knowledge of the structure facilitates studies of the binding and interactions with the activators of Raf-1. These studies will also form the basis for elucidating how this small domain may simultaneously bind several ligands, including Ras and PS. It is clear that there is a dichotomy within this family of domains that divides them into those that bind DAG and those that do not. We have

Table 1. Structural statistics for the 27 final structures of the Raf-1 CRD

RMSDs from experimental restraints	
All NOEs	0.045 (0.0052) Å
Intraresidue NOEs ($ij, j = 1$)	0.043 (0.0009) Å
Sequential NOEs ($ij, j = i + 1$)	0.018 (0.0050) Å
Short-range NOEs ($ij, i + 2 \leq j \leq i + 4$)	0.052 (0.0247) Å
Long-range NOEs ($ij, j \geq i + 5$)	0.054 (0.0091) Å
Hydrogen bonds	0.085 (0.0161) Å
Dihedral angles	0.335 (0.1096)°
RMSDs from ideal geometry	
Bonds	0.006 (0.0002) Å
Angles	0.697 (0.050)°
Impropers	0.614 (0.044)°
Energy	
F_{NOE}*	33.46 (4.58) kcal·mol^{-1}
F_{tor}†	0.437 (0.21) kcal·mol^{-1}
E_{IJ}	−128.1 (6.44) kcal·mol^{-1}
Atomic RMS differences	
Residues 139–184:	
Backbone atoms only	0.926 (0.231) Å
All heavy atoms	1.374 (0.203) Å
Residues 139–145 and 150–176:	
Backbone atoms only	0.441 (0.123) Å
All heavy atoms	1.024 (0.141) Å

The numbers in parentheses are the standard deviations.
*Calculated with a force constant of 50 kcal·mol^{-1}·Å^{-2}.
†Calculated with a force constant of 200 kcal·mol^{-1}·rad^{-1}.

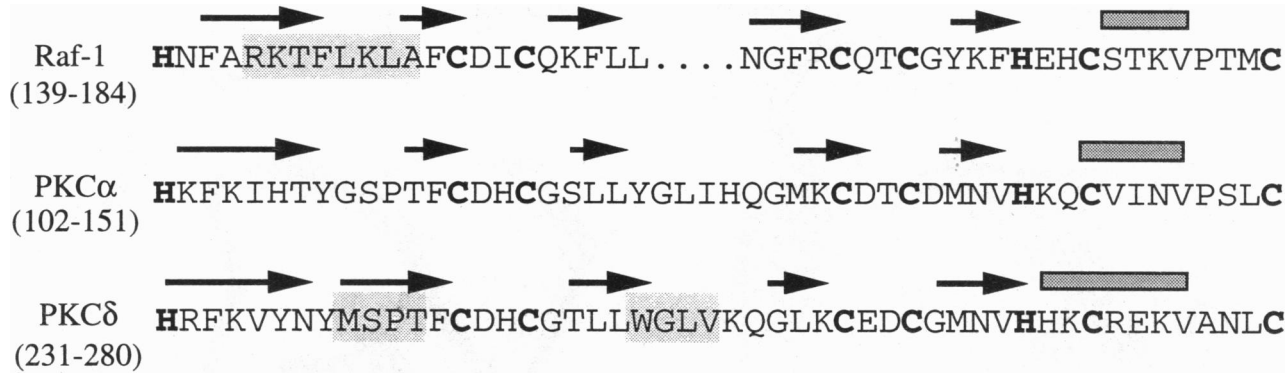

FIG. 4. The sequence alignment of the CRDs from Raf-1 and the PKC α and δ forms. Shown above each sequence is the position of the secondary structure, with the β-strands denoted by arrows and the α-helix by a shaded box. The shaded region in the Raf-1 sequence corresponds to the consensus sequence thought to be involved in Raf-1 activation (50). The shaded regions in the PKC δ sequence correspond to the residues implicated in phorbol ester binding (33).

shown that the difference in specificity of the Raf-1 and PKC domains may be accounted for by a difference in the structure of one of the loops that is critical for the interaction between PKC and its activator, phorbol ester.

The PKC domains are thought to bind phospholipid in a manner that does not compete with the binding of DAG (53), suggesting that the phospholipid binding site is distinct from the phorbol ester/DAG binding site. The binding of phorbol ester to the CRD of PKC δ has been suggested to result in the formation of a contiguous hydrophobic patch that may be involved in plasma membrane insertion (33). This model for membrane insertion is consistent with the hypothesis that this CRD can bind both DAG and PS simultaneously, as both are part of the lipid bilayer. Hence, the binding sites for these activators may be on the same surface of the domain.

Membrane interactions are also involved in the activation of the Raf-1 CRD, which binds the membrane-bound protein Ras and also the phospholipid PS. The binding site for PS may reside in regions of the structure that are conserved in both the Raf-1 and PKC CRDs, since this is a common ligand. Based on our model, the formation of a complex between Ras, PS, and the N terminus of Raf-1 is necessary for activation of the Raf-1 kinase (14, 18). However, in this case, one of the activators (H-Ras) is not inserted into the membrane like PS or DAG, but rather is anchored to the membrane by a lipid moiety on the C terminus. Thus the binding of Ras to the Raf-1 CRD is unlikely to facilitate plasma membrane insertion, and the relative orientation of the Ras/PS binding sites in the Raf-1 domain may be different to the orientation of the DAG/PS binding sites in the PKC domains. The identification of these

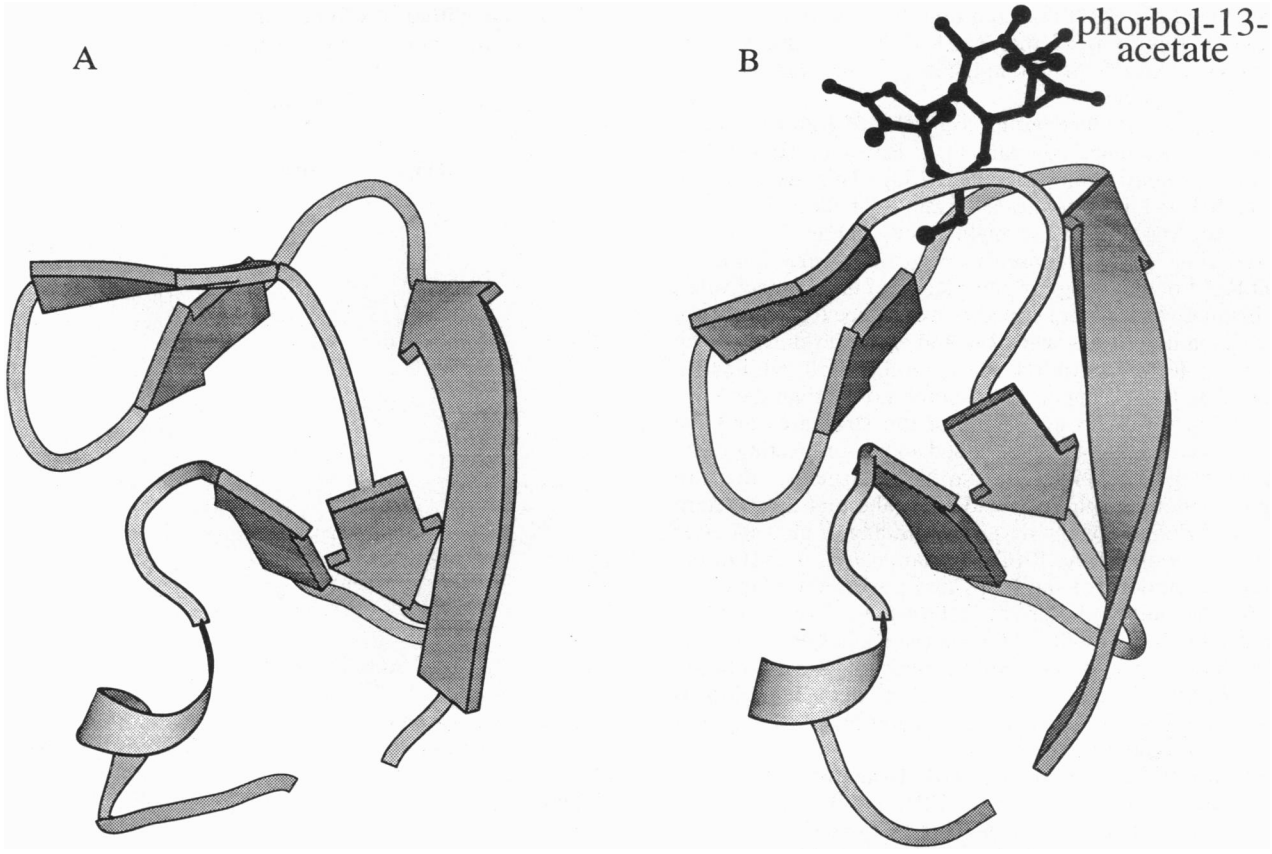

FIG. 5. Comparison of the structures of (*A*) the Raf-1 CRD and (*B*) the PKC δ CRD in a complex with a phorbol ester (33), generated using Molscript (49). One of the loops involved in interacting with phorbol ester in the PKC δ CRD is truncated in the Raf-1 CRD.

binding sites by both NMR and mutagenesis approaches is an effort ongoing in our laboratory.

We thank Paul Barlow for advice on Zn^{2+} restraints, Jonelle Drugan for helpful discussions, and Adrienne Cox, Channing Der, and Roya Khosravi-Far for critical reading of the manuscript, and the Glaxo–Wellcome NMR Group for recording a 3D NOESY. This work was supported by National Institutes of Health Grant RO1 CA70308-1 to S.L.C. and Burroughs Wellcome to S.L.C. and H.R.M.

1. Daum, G., Eisenmann-Tappe, I., Fries, H.-W., Troppmair, J. & Rapp, U. R. (1994) *Trends Biochem. Sci.* **19,** 474–480.
2. Clark, G. J. & Der, C. J. (1993) in *Regulatory GTP Binding Proteins*, eds. Dickey, B. & Birnbaumer, L. (Springer, Heidelberg), pp. 259–287.
3. Crews, C. M. & Erikson, K. L. (1993) *Cell* **74,** 215–217.
4. Avruch, J., Zhang, X. F. & Kyriakis, J. M. (1994) *Trends Biochem. Sci.* **19,** 279–283.
5. Leevers, S. J., Paterson, H. F. & Marshall, C. J. (1994) *Nature (London)* **369,** 411–413.
6. Stokoe, D., Macdonald, S. G., Cadwallader, K., Symons, M. & Hancock, J. F. (1994) *Science* **264,** 1463–1466.
7. Stanton, V. P., Nichols, D. W., Laudano, A. P. & Cooper, G. M. (1989) *Mol. Cell. Biol.* **9,** 639–647.
8. Heidecker, G., Huleihel, M., Cleveland, J. L., Kolch, W., Beck, T. W., Lloyd, P., Pawson, T. & Rapp, U. R. (1990) *Mol. Cell. Biol.* **10,** 2503–2512.
9. Ishikawa, F., Sakai, R., Ochiai, M., Takaku, F., Sugimura, T. & Nagao, M. (1988) *Oncogene* **3,** 653–658.
10. Chuang, E., Barnard, D., Hettich, L., Zhang, X.-F., Avruch, J. & Marshall, M. S. (1994) *Mol. Cell. Biol.* **14,** 5318–5325.
11. Vojtek, A. B., Hollenberg, S. M. & Cooper, J. A. (1993) *Cell* **74,** 205–214.
12. Emerson, S. D., Madison, V. S., Palermo, R. E., Waugh, D. S., Scheffler, J. E., Tsao, K.-L., Kiefer, S. E., Liu, S. P. & Fry, D. C. (1995) *Biochemistry* **34,** 6911–6918.
13. Nassar, N., Horn, G., Herrmann, C., Scherer, A., McCormick, F. & Wittinghofer, A. (1995) *Nature (London)* **375,** 554–560.
14. Ghosh, S., Qin Xie, W., Quest, F. G., Mabrouk, G. M., Strum, J. C. & Bell, R. M. (1994) *J. Biol. Chem.* **269,** 10000–10007.
15. Ghosh, S. & Bell, R. M. (1994) *J. Biol. Chem.* **269,** 30785–30788.
16. Brtva, T. R., Drugan, J. K., Ghosh, S., Terrell, R. S., Campbell-Burk, S., Bell, R. M. & Der, C. J. (1995) *J. Biol. Chem.* **270,** 9809–9812.
17. Hu, C.-D., Kariya, K., Tamada, M., Akasaka, K., Shirouzu, M., Yokoyama, S. & Kataoka, T. (1995) *J. Biol. Chem.* **270,** 30274–30277.
18. Drugan, J. K., Khosravi-Far, R., White, M. A., Der, C. J., Sung, Y.-J., Hwang, Y.-W. & Campbell, S. L. (1996) *J. Biol. Chem.* **271,** 233–237.
19. Freed, E., Symons, M., Macdonald, S. G., McCormick, F. & Ruggieri, R. (1994) *Science* **265,** 1713–1716.
20. Irie, K., Gotoh, Y., Yashar, B. M., Errede, B., Nishida, E. & Matsumoto, K. (1994) *Science* **265,** 1716–1719.
21. Fu, H., Xia, K., Palla, D. C., Cui, C., Conroy, K., Narsimhan, R. P., Mamon, H., Collier, R. J. & Roberts, T. M. (1994) *Science* **266,** 126–129.
22. Fantl, W. J., Muslin, A. J., Kikuchi, A., Martin, J. A., MacNicol, A. M., Gross, R. W. & Williams, L. T. (1994) *Nature (London)* **371,** 612–614.
23. Li, S., Janosch, P., Tanji, M., Rosenfeld, G. C., Waymire, J. C., Mischak, H., Kolch, W. & Sedivy, J. M. (1995) *EMBO J.* **14,** 685–696.
24. Luo, Z.-J., Zhang, X.-F., Rapp, U. & Avruch, J. (1995) *J. Biol. Chem.* **270,** 23681–23687.
25. Chow, Y. H., Pulmiglia, K., Jun, T. H., Dent, P., Sturgill, T. W. & Jove, R. (1995) *J. Biol. Chem.* **270,** 14100–14106.
26. Lu, X., Chou, T.-B., Williams, N. G., Roberts, T. & Perriman, N. (1993) *Genes Dev.* **7,** 621–632.
27. Ono, Y., Fujii, T., Igarashi, K., Takayoshi, K., Tanaka, C., Kikkawa, U. & Nishizuka, Y. (1989) *Proc. Natl. Acad. Sci. USA* **86,** 4868–4871.
28. Lee, J., Ahmed, S., Kozma, R., Teo, M., Monfries, C. & Lim, L. (1992) *Biochem. Soc. Trans.* **20,** 310S.
29. Schaap, D., de Widt, J., van der Wal, J., Vandekerckhove, J., van Damme, J., Gussow, D., Pleogh, H., van Blittenswijk, W. J. & van der Bend, R. L. (1990) *FEBS Lett.* **275,** 151–158.
30. Coppola, J., Bryant, S., Koda, T., Conway, D. & Barbacid, M. (1991) *Cell Growth Differ.* **2,** 95–105.
31. Ahmed, S., Kozma, R., Monfries, C., Harden, N. & Lim, L. (1991) *Biochem. J.* **280,** 233–241.
32. Hommel, U., Zurini, M. & Luyten, M. (1994) *Nat. Struct. Biol.* **1,** 383–387.
33. Zhang, G., Kazanietz, M. G., Blumberg, P. M. & Hurley, J. H. (1995) *Cell* **81,** 917–924.
34. Driscoll, P. C., Clore, G. M. & Marion, D. (1990) *Biochemistry* **29,** 3542–3556.
35. Kay, L. E., Keifer, P. & Saarinen, T. (1992) *J. Am. Chem. Soc.* **114,** 10663–10665.
36. Marion, D., Driscoll, P. C., Kay, L. C., Wingfield, P. T., Bax, A., Gronenborn, A. M. & Clore, G. M. (1989) *Biochemistry* **28,** 6150–6156.
37. Shaka, A. J., Lee, C. J. & Pines, A. (1988) *J. Magn. Reson.* **77,** 274–293.
38. Piotto, M., Saudek, V. & Sklenar, V. (1992) *J. Biomol. NMR* **2,** 661–665.
39. Rance, M., Sorenson, O. W., Bodenhausen, G., Wagner, G., Ernst, R. R. & Wüthrich, K. (1983) *Biochem. Biophys. Res. Commun.* **117,** 479–485.
40. Braunschweiler, L. & Ernst, R. R. (1983) *J. Magn. Reson.* **53,** 521–528.
41. Jeener, J., Meier, B. H., Bachmann, P. & Ernst, R. R. (1979) *J. Chem. Phys.* **71,** 4546–4553.
42. Billeter, M., Neri, D., Otting, G., Qian, Y. Q. & Wüthrich, K. (1992) *J. Biomol. NMR* **2,** 257–274.
43. Mueller, L. (1987) *J. Magn. Reson.* **72,** 191–197.
44. Brunger, A. T. (1992) X-PLOR: *A System for X-ray Crystallography and NMR* (Yale Univ. Press, New Haven, CT).
45. Pelton, J. G., Torchia, D. A., Meadow, N. D. & Roseman, S. (1993) *Protein Sci.* **2,** 543–558.
46. Diakun, G. P., Fairall, L. & Klug, A. (1986) *Nature (London)* **324,** 698–699.
47. Wüthrich, K. (1986) *NMR of Proteins and Nucleic Acids* (Wiley, New York).
48. Blomberg, F., Maurer, W. & Rüterjans, H. (1977) *J. Am. Chem. Soc.* **99,** 8149–8159.
49. Kraulis, P. J. (1993) *J. Appl. Crystallogr.* **24,** 946–950.
50. Clark, G. J., Drugan, J. K., Terrell, R. S., Bradham, C., Der, C. J., Bell, R. M. & Campbell-Burk, S. (1996) *Proc. Natl. Acad. Sci. USA* **93,** 1577–1581.
51. Kazanietz, M. G., Wang, S., Milne, G. W. A., Lewin, N. E., Liu, H. L. & Blumberg, P. M. (1995) *J. Biol. Chem.* **270,** 21852–21859.
52. Newton, A. C. (1995) *J. Biol. Chem.* **270,** 28495–28498.
53. Bell, R. M. & Burns, D. J. (1991) *J. Biol. Chem.* **266,** 4661–4664.